Ab Initio Conformational and Stereopermutational Analysis of Dihydroxyphosphoranyl, $H_2P(OH)_2$

Christopher J. Cramer* and Susan M. Gustafson

Contribution from the Department of Chemistry and Supercomputer Institute, University of Minnesota, 207 Pleasant Street SE, Minneapolis, Minnesota 55455-0431

*Received September 22, 1993**

Abstract: The potential energy hypersurface for $H_2P(OH)_2$ has been explored at correlated levels. Seven local minima and 29 different stereopermutational transition states interconnecting them were located. The transition states correspond to internal rotation, pseudorotation, double pseudorotation, and pseudoinversion. The stereochemical consequences of these processes are analyzed in detail as is the nature of the singly occupied molecular orbital throughout. Geometric and natural bond orbital analyses indicate the importance of hyperconjugative interactions through phosphorus in stabilizing various kinds of stationary points. The latter effect is maximized for the interaction of equatorial substituents in the trigonal-bipyramidal phosphoranyl minima. Comparison to closed shell phosphoranes and monohydroxy- and other phosphoranyl radicals is provided. Dihydroxyphosphoranyl is predicted to possibly be stable to homolytic decomposition under suitable conditions and calculated electron spin resonance and infrared spectral data are provided.

Introduction

Organophosphorus compounds are ubiquitous in (1) living systems, where they are the chief currency of biological energy transactions,[1,2] (2) the environment, where they find use as pesticides, fertilizers, and chemical warfare agents,[3,4] and (3) synthetic organic chemistry, where phosphorus-based functionalities are used to impart chirality and/or reactivity.[5-9] Stereochemical issues are often key to the properties exhibited by these various molecules. For instance, basic aqueous phosphate hydrolysis is usually assumed to involve the intermediacy of an anionic phosphorane arising from hydroxide addition to phosphorus.[10-13] The pentacoordinate, trigonal-bipyramidal phosphorane has two stereochemically distinct groups of substituents: two axial and three equatorial. Since addition and elimination (i.e., hydrolysis) are presumed to occur apically in TBP systems,[14-16] stereopermutation may be required to move the desired leaving group from an equatorial to an axial position. Berry pseudorotation, which will later be discussed in more detail, is the well-known process most typically invoked to accomplish this.[17-22]

In organic synthesis, on the other hand, phosphorus-based stereochemistry finds use in the creation of chiral prosthetic groups which induce chirotopicity at nearby reacting centers. One example of particular interest to us is the degree to which the orientation of a carbanion is controlled by the stereochemistry of an attached phosphonic acid derivative. In particular, it has been noted that atoms attached to phosphorus which bear lone pairs of electrons, including carbanions, tend to orient themselves so as to take maximal advantage of opportunities for hyperconjugative stabilization.[6,23] That is, each lone pair on an atom Y tends to be antiperiplanar to a low-energy σ^*_{PX} antibonding acceptor orbital resulting in a stabilizing $n_Y \rightarrow \sigma^*_{PX}$ delocalization. This kind of hyperconjugative stabilization, which was first noted in the context of the stabilization of axial sugar anomers, is now typically referred to as the *generalized anomeric effect*.[24] This effect is operative in all manner of phosphorus compounds, to include phosphates and the phosphorane hydrolysis intermediates discussed above.[13,25,26] Moreover, it appears to play a key role in the open-shell analogs of phosphoranes, the so-called phosphoranyl radicals.[27-45]

Phosphoranyl radicals offer both a practical and an aesthetic

* Abstract published in *Advance ACS Abstracts*, December 15, 1993.

(1) Westheimer, F. H. *Science* **1987**, *237*, 1173.
(2) Erecinska, M.; Wilson, D. F. *Trends Biochem. Sci.* **1978**, *3*, 219.
(3) Avila, L. Z.; Loo, S. H.; Frost, J. W. *J. Am. Chem. Soc.* **1987**, *109*, 6758.
(4) *Organophosphorus Pesticides: Organic and Biological Chemistry*; Eto, M., Ed.; CRC Press: Cleveland, 1974.
(5) Denmark, S. E.; Marlin, J. E. *J. Org. Chem.* **1987**, *52*, 5742.
(6) Cramer, C. J.; Denmark, S. E.; Miller, P. C.; Dorow, R. L.; Swiss, K. A.; Wilson, S. R. *J. Am. Chem. Soc.* Submitted for publication.
(7) Hanessian, S.; Bennani, Y. L. *Tetrahedron Lett.* **1990**, *31*, 6465.
(8) Vasella, A.; Voeffray, R. *Helv. Chim. Acta* **1982**, *65*, 1953.
(9) Denmark, S. E.; Cramer, C. J. *J. Org. Chem.* **1990**, *55*, 1806.
(10) Taira, K.; Uchimaru, T.; Storer, J. W.; Yliniemela, A.; Uebayasi, M.; Tanabe, K. *J. Org. Chem.* **1993**, *58*, 3009.
(11) Dejaegere, A.; Lim, C.; Karplus, M. *J. Am. Chem. Soc.* **1991**, *113*, 4353.
(12) Setzer, W. N.; Bentrude, W. G. *J. Org. Chem.* **1991**, *56*, 7212.
(13) Lim, C.; Tole, P. *J. Phys. Chem.* **1992**, *96*, 5217.
(14) Lohr, L. L. *J. Phys. Chem.* **1984**, *88*, 5569.
(15) Hay, R. S.; Roberts, B. P. *J. Chem. Soc., Perkin Trans. 2* **1978**, 770.
(16) Bentrude, W. G. *Acc. Chem. Res.* **1982**, *15*, 117.
(17) Berry, R. S. *J. Chem. Phys.* **1960**, *32*, 933.
(18) Luckenbach, R. *Dynamic Stereochemistry of Pentacoordinated Phosphorus and Related Elements*; Georg Thieme: Stuttgart, 1973.
(19) Russegger, P.; Brickmann, J. *Chem. Phys. Lett.* **1975**, *30*, 276.
(20) Ugi, I.; Marquarding, D.; Klusacek, H.; Gillespie, P.; Ramirez, F. *Acc. Chem. Res.* **1971**, *4*, 288.
(21) Mislow, K. *Acc. Chem. Res.* **1970**, *3*, 321.
(22) Wang, P.; Agrafiotis, D. K.; Streitwieser, A.; Schleyer, P. v. R. *J. Chem. Soc., Chem. Commun.* **1990**, 201.
(23) Zarges, W.; Marsch, M.; Harns, K.; Haller, F.; Frenking, G.; Boche, G. *Chem. Ber.* **1991**, *124*, 861.
(24) Reed, A. E.; Schleyer, P. v. R. *J. Am. Chem. Soc.* **1987**, *109*, 7362.
(25) Wang, P.; Zhang, Y.; Glaser, R.; Streitwieser, A.; Schleyer, P. v. R. *J. Comput. Chem.* **1993**, *14*, 522.
(26) Wang, P.; Zhang, Y.; Glaser, R.; Reed, A. E.; Schleyer, P. v. R.; Streitwieser, A. *J. Am. Chem. Soc.* **1991**, *113*, 55.
(27) Cramer, C. J. *J. Am. Chem. Soc.* **1990**, *112*, 7965.
(28) Cramer, C. J. *J. Am. Chem. Soc.* **1991**, *113*, 2439.
(29) Cramer, C. J. *Chem. Phys. Lett.* **1993**, *202*, 7034.
(30) Cramer, C. J.; Famini, G. R. *J. Am. Chem. Soc.* **1990**, *112*, 5460.
(31) Cramer, C. J.; Famini, G. R. *Chem. Phys. Lett.* **1990**, *169*, 405.
(32) Cramer, C. J.; Gustafson, S. M. *J. Am. Chem. Soc.* **1993**, *115*, 9315.
(33) Aagaard, O. M.; Janssen, R. A. J.; de Waal, B. F. M.; Buck, H. M. *J. Am. Chem. Soc.* **1990**, *112*, 938.
(34) Schipper, P.; Jansen, E. H. J. M.; Buck, H. M. *Top. Phosphorus Chem.* **1977**, *9*, 407.
(35) Hay, R. S.; Roberts, B. P.; Singh, K.; Wilkinson, J. P. T. *J. Chem. Soc., Perkin Trans. 2* **1979**, 756.
(36) Hamerlinck, J. H. H.; Schipper, P.; Buck, H. M. *J. Am. Chem. Soc.* **1983**, *105*, 385.
(37) Roberts, B. P. *Tetrahedron Lett.* **1983**, *24*, 3377.
(38) Janssen, R. A. J.; Kingma, J. A. J. M.; Buck, H. M. *J. Am. Chem. Soc.* **1988**, *110*, 3018.
(39) Janssen, R. A. J.; Sonnemans, M. H. W.; Buck, H. M. *J. Chem. Phys.* **1986**, *84*, 3694.
(40) Janssen, R. A. J.; Buck, H. M. *Chem. Phys. Lett.* **1986**, *132*, 459.

0002-7863/94/1516-0723$04.50/0

Chart 1

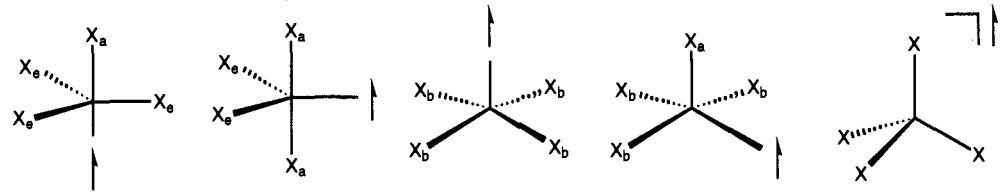

TBP_a **TBP_e** **SP_a** **SP_b** **DT**

allure. In the practical sense, they are implicated as metastable intermediates in the biodegradation of toxic organophosphorus compounds,[3] although the mechanism of their production remains unclear. They also are produced when genetic material is exposed to ionizing radiation.[16,33] An understanding of the fundamental characteristics which impart stability to these radicals may thus assist in the design of more or less robust closed-shell precursors, depending on the desired properties of the latter. All of the stereochemical considerations discussed above are intimately associated with compound conformation and stability, and the diversity of structures which arise are particularly fascinating in the open-shell case. The five most important idealized phosphoranyl radical geometries that we will use in later discussion are illustrated in Chart I. If one views the unpaired electron as a fifth "substituent", the trigonal-bipyramidal (TBP) and square-pyramidal (SP) stereostructures are familiar from phosphorane chemistry. Because of the unique nature of the unpaired electron, each of these two geometries is further defined by the localization of the radical, either equatorial (TBP_e) or axial (TBP_a) in the trigonal bipyramid or apical (SP_a) or basal (SP_b) in the square pyramid. Finally, there is certainly no requirement that the unpaired electron really resemble a substituent. If instead it is predominantly localized in some antibonding molecular orbital (MO), the phosphoranyl radical may adopt what amounts to a distorted tetrahedral (DT) geometry, also sometimes called a σ^* geometry by reference to the MO picture.

Experimentally, electron spin resonance (ESR) spectroscopy suggests that the majority of phosphoranyl radicals exist as TBP_e structures.[34] Various examples of DT[35] and TBP_a[36] geometries have also appeared in the literature, although the latter have been few and controversial.[37] Theory, which in addition to predicting equilibrium geometries may also be used to predict ESR coupling constants, is in general accord with experimental data with regard to the prevalence of TBP_e structures.[28,29,38-44] Only recently, for the particular case of $HP(OH)_3$, has a TBP_a local minimum been predicted for *any* phosphoranyl radical.[32] Of course, one should keep in mind that structures intermediate between the idealized geometries illustrated in Chart 1 are perfectly allowed, and indeed the phosphoranyl radical anion PCl_2FS appears to adopt a geometry midway between TBP_e and DT.[40]

Because of the biological prevalence of phosphate and phosphonate esters and their derivatives, we have been particularly interested in developing a greater understanding of the stereochemical details of phosphoranyl radicals substituted with hydroxyl groups. To that end, we have explored in some detail the potential energy hypersurface of monohydroxyphosphoranyl, $H_3P(OH)$.[27] In addition to locating two TBP_e local minima, one with the hydroxyl group axial and the other equatorial, several modes of isomerization were examined. Pseudoinversion, a stereopermutation which exchanges the two axial and two equatorial ligands in the TBP_e geometry while simultaneously inverting the unpaired electron through the central phosphorus atom, was determined to be the lowest energy pathway interconverting the two TBP_e isomers. This pathway is obviously unavailable to phosphoranes.

Somewhat higher energy pseudorotation pathways were also explored. In a TBP, pseudorotation involves holding one of the equatorial substituents in a fixed position. The other two equatorial substituents (which ideally are related by a bond angle of 120°) and the two axial substituents (which ideally are related by a bond angle of 180°) are then simultaneously bent away from each other and toward each other, respectively. When the two different bond angles are both 150°, one arrives at the SP geometry in which the substituent of the TBP which was held fixed is now the apical substituent of the SP. In phosphoranes, this structure is typically the transition state between different TBP local minima. In phosphoranyl *radicals*, on the other hand, the unpaired electron is so *apicophobic* that TBP_a structures, arising from the equatorial unpaired electron being pseudorotated into an axial position through a SP_b intermediate, are *not in general stationary*. Instead, the SP_b transition states (TSs) lead directly to TBP_e structures in both directions. In *closed shell* TBPs, assuming the ideal least motion pathway, it is not possible for a basal substituent in the SP TS to both begin and end a pseudorotation in an equatorial position. In order to accomplish such a permutation, a second formal pseudorotation would be required. We now call this *open-shell* process, which interconverts two TBP_e minima via an SP_b transition state, a "double pseudorotation", and it was found to be operative in H_3POH.

Finally, pseudorotations were characterized in which the equatorially disposed unpaired electron served as the fixed substituent in the TBP, i.e., occurring through a SP_a intermediate. While this process now resembles the simpler phosphorane case, since the unpaired electron is not moved from an equatorial position when apical on the SP, it is the highest energy stereopermutation for H_3POH. The situation is quite similar for the thiol analog, H_3PSH.[29,45]

One interesting trend observed for all of the stationary points on the H_3POH hypersurface was that in every case the adopted geometries took maximal advantage of $n_O \rightarrow \sigma^*_{PH}$ hyperconjugative stabilization. Wang and co-workers have examined mono- and disubstituted hydroxyphosphoranes and made similar observations.[25,26] Of particular note is that the generalized anomeric effect through phosphorus appears to be considerably more stabilizing for the lone pair on an equatorially disposed substituent atom delocalizing into an equatorially disposed acceptor orbital. For instance, in TBP_e difluorophosphoranyl, H_2PF_2, the cost of moving the first fluorine from its preferred axial position to an equatorial one is considerably greater than the second, because of the strong eq–eq hyperconjugative stabilization available in the doubly equatorial isomer.[28] Similar effects are observed in di- and trihydroxyphosphorane and trihydroxyphosphoranyl, i.e., hyperconjugation competes with apicophilicity.[32]

In order to gain more insight into the nature of interactions between phosphoranyl substituents, both hyperconjugative and otherwise, we present here an exhaustive analysis of the potential

(41) Aagaard, O. M.; de Waal, B. F. M.; Cabbolet, M. J. T. F.; Janssen, R. A. J. *J. Phys. Chem.* **1992**, *96*, 614.
(42) Geoffroy, M.; Rao, G.; Tančič, Z. Bernardinelli, G. *J. Am. Chem. Soc.* **1990**, *112*, 2826.
(43) Janssen, R. A. J.; Visser, G. J.; Buck, H. M. *J. Am. Chem. Soc.* **1984**, *106*, 3429.
(44) Colussi, A. J.; Morton, J. R.; Preston, K. F. *J. Phys. Chem.* **1975**, *79*, 1855.
(45) Gonbeau, D.; Guimon, M.-F.; Ollivier, J.; Pfister-Guillouzo, G. *J. Am. Chem. Soc.* **1986**, *108*, 4760.

Table 1. Relative Energies for $H_2P(OH)_2$ at Various Levels of Theory[a,b]

structure	symmetry	UHF	MP2	MP4//MP2
$aa1_m$	C_s	0.0	0.0	0.0
$aa2_m$	C_2	0.2	0.5	0.4
aa1*	C_1	0.8	1.3	1.3
aa2*	C_1	4.3	5.6	5.7
$ee1_m$	C_2	2.6	4.7	4.5
$ee2_m$	C_s	3.5	5.5	5.3
ee1*	C_1	8.5	11.8	11.4
ee2*	C_1	7.4	10.8	10.3
$ae1_m$	C_1	1.8	3.6	3.5
$ae2_m$	C_1	4.8	6.7	6.4
$ae3_m$	C_1	6.2	8.3	8.0
$ae4_m$	C_1	5.3	*c*	*c*
ae1*	C_1	10.1	12.2	12.1
ae2*	C_1	9.2	11.8	11.5
ae3*	C_1	6.4	8.5	8.2
ae4*	C_1	5.3	*c*	*c*
ae5*	C_1	8.5	10.8	10.4
ae6*	C_1	8.9	10.5	9.9
$\psi_{inv}1$	C_s	25.1	21.4	20.9
$\psi_{inv}2$	C_2	24.5	20.7	20.2
$\psi_{inv}3$	C_1	23.9	21.2	20.9
$\psi_{inv}4$	C_2	26.7	23.0	22.4
$\psi_{inv}5$	C_2	25.4	23.1	22.9
$\psi_{rot}1$	C_s	16.5	14.5	14.7
$\psi_{rot}2$	C_2	16.1	14.0	14.2
$\psi_{rot}3$	C_1	20.0	19.4	19.4
$\psi_{rot}4$	C_s	25.4	24.4	24.2
$\psi_{rot}5$	C_s	25.1	25.0	24.9
$\psi_{rot}^{dbl}1$	C_1	11.4	13.1	13.0
$\psi_{rot}^{dbl}2$	C_1	12.0	13.9	13.7
$\psi_{rot}^{dbl}3$	C_1	11.6	12.3	12.4
$\psi_{rot}^{dbl}4$	C_s	7.5	8.1	8.1
$\psi_{rot}^{dbl}5$	C_s	9.2	10.5	10.7
$\psi_{rot}^{dbl}6$	C_s	10.5	11.4	11.3
$\psi_{rot}^{dbl}7$	C_1	12.3	13.1	12.8
$\psi_{rot}^{dbl}8$	C_1	10.1	10.3	9.8
$\psi_{rot}^{dbl}9$	C_1	10.5	10.8	10.6
$\psi_{rot}^{dbl}10$	C_1	15.0	16.4	16.1
$OP(OH)H_2 + H$		1.7	2.6	5.0
$P(OH)_2H + H$		6.6	10.0	10.3
$P(OH)H_2 + OH$		9.3	41.7	38.9

[a] Kcal/mol. [b] All levels employ the 6-31G* basis set. Excitations from core orbitals were included in MP4 treatment. Absolute energy (au) of $aa1_m$ is HF, −492.71129; MP2, −493.18095; MP4//MP2, −493.23177. [c] Not stationary at levels above UHF.

energy hypersurface for the open-shell $H_2P(OH)_2$. We focus on enumerating all local minima, and all stereopermutational pathways interconnecting them. We examine in particular stereoelectronic effects operating in both minima and transition states using both geometrical and natural bond orbital (NBO)[46] population analyses. Finally, we provide calculated ESR hyperfine coupling constants (hfs) and infrared frequencies as supplementary material.

Computational Methods

All calculations employed the 6-31G* basis set.[47] All open-shell geometries were fully optimized at the UHF and UMP2 levels of theory, while closed shell geometries used the corresponding restricted levels.[48] Spin contamination was negligible in all instances, with values of $\langle S^2 \rangle$ ranging from 0.75 to 0.77. The effects of correlation were examined via single point calculations at the MP4 level with excitations of core electrons included for the MP2 (frozen core) geometries. Vibrational frequencies were calculated under the rigid-rotor, harmonic oscillator approximation at the UHF level for all stationary points;[48] local minima and transition-state structures were confirmed to have exactly zero and one imaginary frequencies, respectively. For each transition state giving rise to a stereopermutation, the intrinsic reaction coordinate[49] was calculated at the UHF level of theory in order to determine the corresponding reactants and products and the minimum energy path connecting them. Hyperconjugative delocalization was examined by second-order perturbation analysis of the off-diagonal Fock matrix elements in the natural bond orbital (NBO) basis. Hyperconjugation is measured in terms of bond or lone pair delocalizations into antibonding orbitals (i.e., $\sigma \rightarrow \sigma^*$ or $n \rightarrow \sigma^*$) and their energetic contribution to the overall electronic structure relative to the idealized Lewis structure. Application of NBO analysis to hyperconjugation in TBP systems has been previously described.[46]

Molecular orbital depictions of the singly occupied molecular orbital (SOMO) are presented as planar slices taken from the appropriate UHF α eigenvector. Isotropic ESR hyperfine coupling constants a_X were calculated in the standard way using

$$a_X = (8\pi/3) g g_X \beta \beta_X \rho(X) \quad (1)$$

$$\rho(X) = \sum_{\mu\nu} P_{\mu\nu}^{\alpha-\beta} \phi_\mu(\boldsymbol{R}_X) \phi_\nu(\boldsymbol{R}_X) \quad (2)$$

where g (g_X) is the electronic (nuclear) g factor, β (β_X) is the Bohr (nuclear) magneton, and the Fermi contact integral, $\rho(X)$, was evaluated from the UMP2 one-electron spin density matrix with excitation of the core electrons included. The UMP2 density matrix enjoys less spin contamination than does the UHF and has the further advantage that it includes some static correlation effects. The electronic g factor was taken to be 2.0 for all cases.

All calculations employed either the GAUSSIAN 92[50] or GAMESS[51] program suites. The former was used for the calculation of all MP2 Fermi contact values, while the latter was used for the generation of all SOMO graphics. A complete listing of archive files for all structures optimized at the MP2 level of theory is provided as supplementary material, as are the calculated ESR and IR spectral data.

Nomenclature. For ease of notation, we will identify structures in the following manner. All local minima are of overall structure TBP_e. They will be indicated by a prefix of either aa, ae, or ee, where the first implies the two hydroxyl groups to both be axial, the second implies one axial and one equatorial, and for the last both are equatorial. The prefix will be followed by a number, reflecting the order in which the structures are presented in the text. Finally, the subscript m will be added to indicate that the structure is a local minimum. Transition states for hydroxyl group rotations which connect the various TBP_e structures will be identified in exactly the same fashion, except that the superscript ‡ will be used instead of the subscript m. For example, $aa1^‡$ will be the first rotational transition state discussed for the TBP_e system in which both hydroxyl groups are axial. Other types of transition states will be uniquely identified by the following prefixes: ψ_{rot} for pseudorotation, ψ_{rot}^{dbl} for double-pseudorotation, and ψ_{inv} for pseudoinversion. Again, the prefix will be followed by a number reflecting the ordinal occurrence of the particular TS in the discussion. In gross structure, ψ_{rot} TSs have SP_a geometries, ψ_{rot}^{dbl} TSs have SP_b geometries (which may closely resemble TBP_a), and ψ_{inv} TSs have geometries roughly intermediate between square planar and DT. Numerous figures are provided to assist in visualization.

Results

The equilibrium geometries of the ground-state dihydroxyphosphoranyl radicals are all trigonal-bipyramidal with the unpaired electron in the equatorial position (TBP_e). The two hydroxyl groups distribute themselves between the two axial and two equatorial positions to generate three possible substitution patterns: axial–axial, equatorial–equatorial and axial–equatorial. For each substitution pattern, there are several isomers related

(46) Reed, A. E.; Curtiss, L. A.; Weinhold, F. *Chem. Rev.* **1988**, *88*, 899.
(47) Francl, M. M.; Pietro, W. J.; Hehre, W. J.; Binkley, J. S.; Gordon, M. S.; DeFrees, D. J.; Pople, J. A. *J. Chem. Phys.* **1982**, *76*, 2161.
(48) Hehre, W. J.; Radom, L.; Schleyer, P. v. R.; Pople, J. A. *Ab Initio Molecular Orbital Theory*; Wiley: New York, 1986.
(49) Gonzalez, C.; Schlegel, H. B. *J. Chem. Phys.* **1989**, *90*, 2154.
(50) Frisch, M. J.; Trucks, G. W.; Head-Gordon, M.; Gill, P. M. W.; Wong, M. W.; Foresman, J. B.; Johnson, B. G.; Schlegel, H. B.; Robb, M. A.; Replogle, E. S.; Gomperts, R.; Andres, J. L.; Raghavachari, K.; Binkley, J. S.; Gonzalez, C.; Martin, R. L.; Fox, D. J.; Defrees, D. J.; Baker, J.; Stewart, J. J. P.; Pople, J. A., GAUSSIAN92, Revision D; Gaussian, Inc.: Pittsburgh, PA.
(51) Schmidt, M. W.; Baldridge, K. K.; Boatz, J. A.; Elbert, S. T.; Gordon, M. S.; Jensen, J. H.; Koseki, S.; Matsunaga, N.; Nguyen, K. A.; Su, S.; Windus, T. L.; Dupuis, M.; Montgomery, J. A., Jr. *J. Comput. Chem.* **1993**, *14*, 1347.

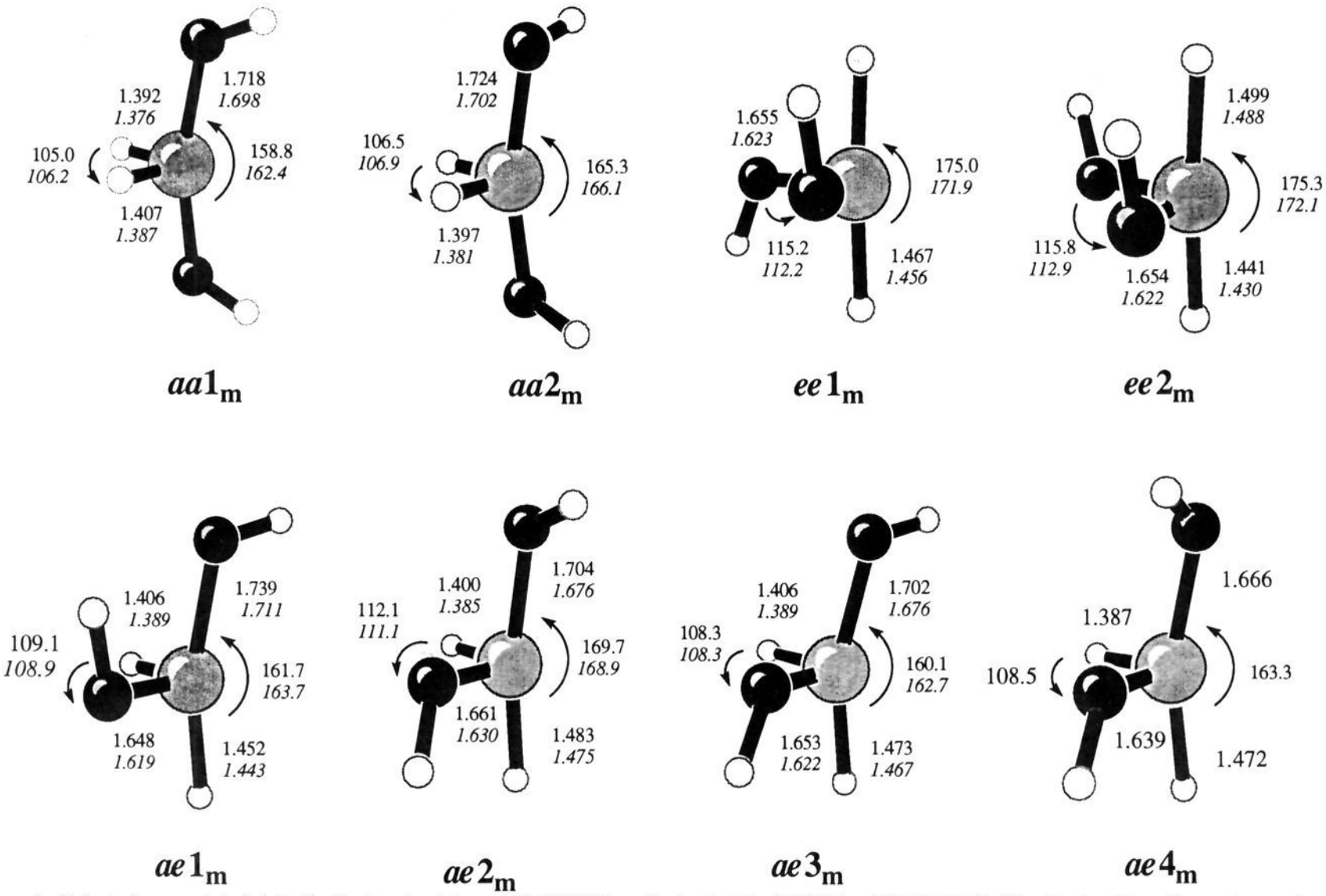

Figure 1. Selected geometrical data for the local minima of $H_2P(OH)_2$ optimized at the UMP2 and UHF (italics) levels; bond lengths are in angstroms and bond angles in deg. Structure $ae4_m$ is not stationary at the UMP2 level.

by hydroxyl group rotation through transition states which interconnect them. Such a rotational process does *not* change the overall stereochemistry of the TBP_e substitution, aa, ae, or ee. There are additionally, on the other hand, a large number of pseudorotation, double-pseudorotation, and pseudoinversion transition states which *do* interconvert the possible TBP_e substitution patterns. The relative energies of all stationary points are collected in Table 1.

Local Minima and Rotational Transition States. The hydroxyl group prefers the apical position in H_3POH by 5.8 kcal/mol.[27] Consistent with this, the global minimum structure for $H_2P(OH)_2$ ($aa1_m$) has both hydroxyl substituents in axial positions. The two O–H bonds are parallel in this isomer, giving rise to a structure of C_s symmetry. There is an additional aa local minimum of C_2 symmetry ($aa2_m$) only 0.4 kcal/mol higher in energy (Figure 1).[52] Just as in axially hydroxyl-substituted H_3POH, the hydroxyl groups orient so that the O–H bond is staggered between an equatorial P–H bond and the axis of the orbital containing the unpaired electron. (Analysis of the rotational coordinate in H_3POH demonstrated this orientation to be dictated predominantly in order to minimize the overall dipole moment.) These two isomers are connected by rotation of one hydroxyl group over either a shorter path of about 120° or a longer one of about 240°. The corresponding C_1 transition states are $aa1^{\ddagger}$ and $aa2^{\ddagger}$, respectively (Figure 2). Again as observed in H_3POH, eclipsing of the unpaired electron by the O–H bond is not particularly costly, with a rotational barrier of 1.3 kcal/mol; however, the alternative pathway has a higher barrier of 5.7 kcal/mol. Figure 3 illustrates the SOMO for $aa1_m$, showing the expected equatorial localization of the radical in a fairly diffuse orbital. Figure 3 also illustrates the SOMO for $aa2^{\ddagger}$.

Four local minima were located with C_1 symmetry for the axial–equatorial substitution pattern (Figure 1). In the lowest energy isomer ($ae1_m$) the equatorial hydroxyl group eclipses the axial P–O bond. As in the aa case, the axial hydroxyl prefers to be oriented gauche to the unpaired electron. There is a single C_1 rotational barrier of 8.6 kcal/mol for axial hydroxyl rotation through $ae1^{\ddagger}$ (Figure 2). The alternative gauche orientation is not a minimum in this case, probably because of the unfavorable interactions with the other hydroxyl group which give rise to the high rotational barrier.

The other three ae isomers, with the equatorial hydroxyl group eclipsing the axial P–H bond, are related by rotations of the axial hydroxyl group. Just as in the aa series, that rotation delivers two local minima ($ae2_m$ and $ae3_m$) for the two possible axial hydroxyl orientations gauche to the unpaired electron. In addition, at the HF level, there appears to be sufficient ionic interaction between the axial hydroxyl proton and the equatorial oxygen to deliver a fourth local minimum ($ae4_m$) in which the axial O–H eclipses the equatorial P–O bond. However, the dimpling of the rotational hypersurface is extremely slight: while the rotational barriers associated with $ae2^{\ddagger}$ and $ae3^{\ddagger}$ are clearly higher in energy than their nearby minima, that is not the case for $ae4^{\ddagger}$, which lies within 0.01 kcal/mol of $ae4_m$. Not surprisingly then, at the MP2 level of theory $ae4_m$ and $ae4^{\ddagger}$ are no longer stationary. Moreover, at all levels of theory the energy difference between $ae3_m$ and $ae3^{\ddagger}$ is less than 0.2 kcal/mol, illustrating again the fairly flat nature of the hypersurface in regions where O–H is eclipsing the unpaired electron. Two last rotational transition states ($ae5^{\ddagger}$ and $ae6^{\ddagger}$) were additionally located which interconvert $ae1_m$ and $ae2_m$ by rotation of the equatorial hydroxyl group. In each of these transition states, the hydroxyl group eclipses one of the other two equatorial positions.

Finally, two local minima were located for diequatorial hydroxyl substitution (Figure 1). The C_2 anti orientation of hydroxyl groups ($ee1_m$) is favored over the C_s syn ($ee2_m$) by 0.8 kcal/mol. Interconversion between the ground-state structures can occur via outward ($ee1^{\ddagger}$) or inward ($ee2^{\ddagger}$) rotation of one hydroxyl

(52) For discussion purposes, unless otherwise stipulated all energies refer to MP4/6-31G*//MP2/6-31G*.

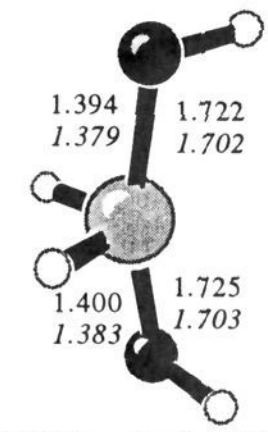

HOPH = 131.7, *130.1*

***aa1*‡**

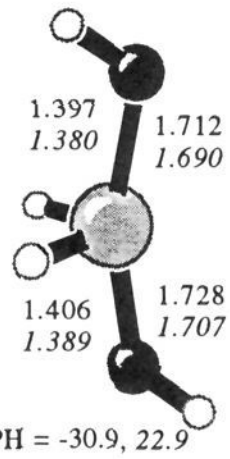

HOPH = -30.9, *22.9*

***aa2*‡**

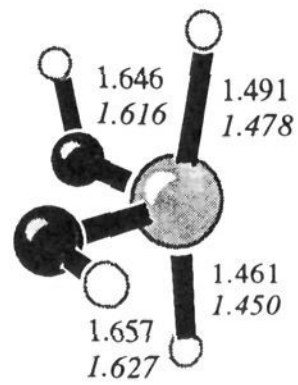

HO_ePO_e = 178.1, *178.1*

***ee1*‡**

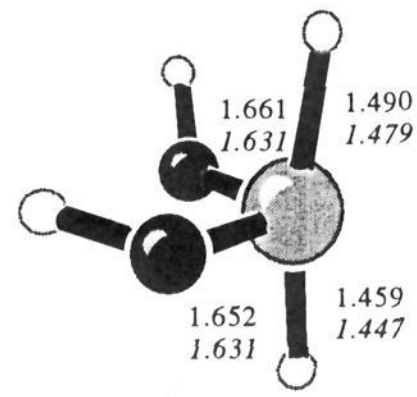

HO_ePO_e = -13.31, *-14.1*

***ee2*‡**

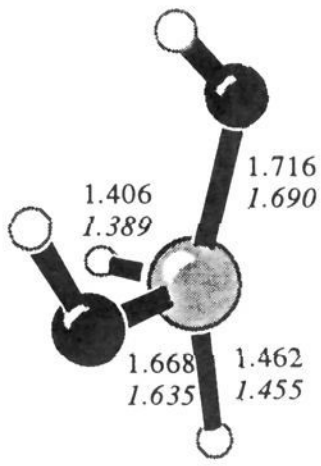

HO_aPO_e = 17.9, *14.3*

***ae1*‡**

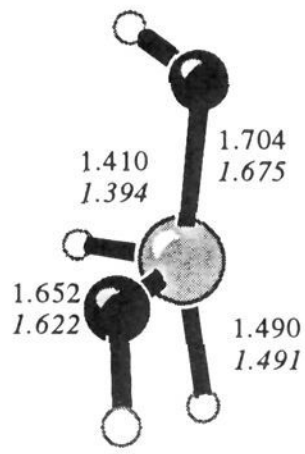

HO_aPH_e = -0.7, *-4.3*

***ae2*‡**

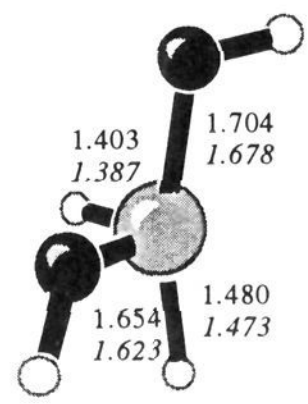

HO_aPH_e = 116.7, *117.1*

***ae3*‡**

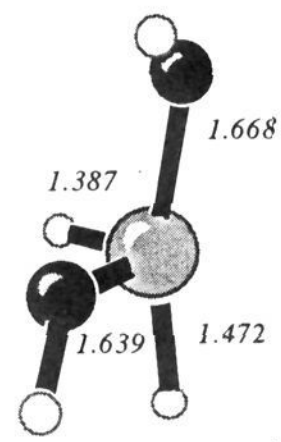

HO_aPH_e = *116.6*

***ae4*‡**

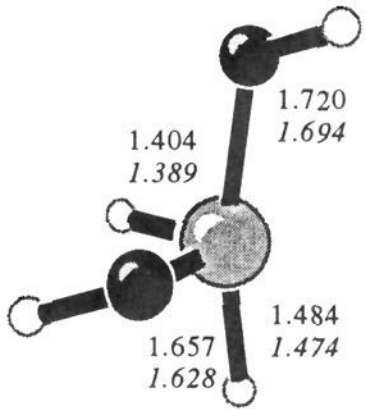

HO_ePH_e = 18.5, *14.3*

***ae5*‡**

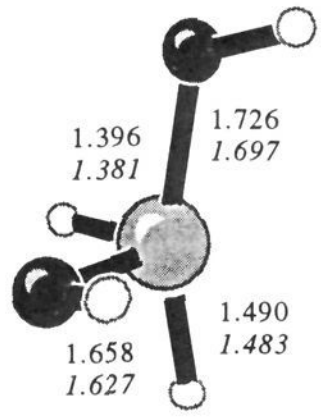

HO_ePH_e = -168.5, *178.4*

***ae6*‡**

Figure 2. Selected geometrical data for hydroxyl group rotational transition state structures of $H_2P(OH)_2$ optimized at the UMP2 and UHF (italics) levels; bond lengths are in angstroms and bond angles in deg. Structure ae4‡ is not stationary at the UMP2 level.

group relative to the other. The inward pathway, which permits some nonideal hydrogen bonding, is favored.

All of the local minima conformed to general trends observed in TBP_e radicals, i.e., axial bonds are bent over slightly towards the unpaired electron and axial bond lengths are typically 0.05–0.1 Å longer than equatorial ones.

Pseudoinversions. Five stationary points with flattened tetrahedral structures were found, each with one imaginary frequency in the 1400–1600*i* cm^{-1} range (Figure 4). These transition-state structures lie 20–23 kcal/mol above $aa1_m$ in energy and correspond to a pseudoinversion process in which both axial substituents are moved to equatorial positions and vice versa. Concomitantly, the unpaired electron inverts through phosphorus, remaining equatorial in the TBP. Figure 5 illustrates this process for C_s $\psi_{inv}1$, which is the transition state for a pseudoinversion linking $aa1_m$ and $ee2_m$, by following the intrinsic reaction coordinate (IRC) linking all three. In addition, Figure 3 illustrates the SOMO for $\psi_{inv}1$, which shows the unpaired electron roughly midway through the inversion process. Although antibonding interactions with the oxygen lone pairs displace the unpaired electron density slightly to the opposite side of the phosphorus atom, the contributing orbital hybrid at phosphorus is quite clearly almost pure p. The nature of the remaining pseudoinversion transition states will be considered in more detail in the discussion section.

It is noteworthy that the barriers to pseudoinversion are 7–8 kcal/mol higher in energy for $H_2P(OH)_2$ than are those for H_3POH.[27] This is entirely consistent with the general trend observed for atoms substituted with an increasing number of electron withdrawing groups, e.g., NF_3 has a much higher inversion barrier than NH_3.[53] This is rationalized by noting that the central atom is forced to remove all s character from the orbital containing the nonbonding electron(s) in the transition state and instead must distribute it into the bonds to its more electronegative substituents.

Pseudorotation. Like pseudoinversion, a pseudorotation (in which the unpaired electron occupies the apical position in the

(53) Bent, H. A. *Chem. Rev.* **1961**, *61*, 275.

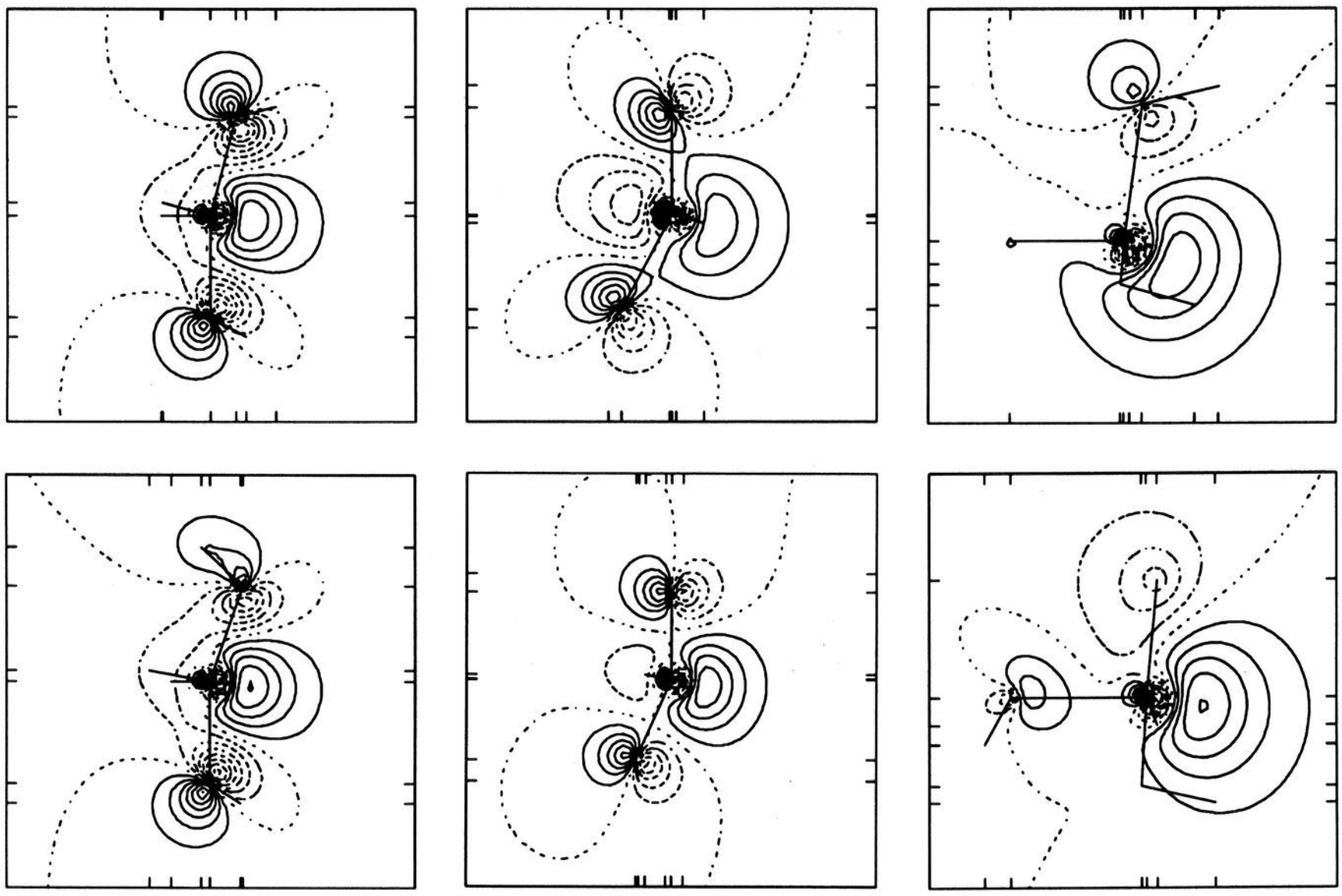

Figure 3. Contour diagrams (0.05 au) of a planar slice through the SOMO for various $H_2P(OH)_2$ stationary points. Upper left: $aa1_m$, TBP_e, OPO plane; lower left: $aa2^{\ddagger}$, TBP_e, OPO plane; upper center: $\psi_{inv}1$, flattened DT, OPO plane; lower center: $\psi_{rot}1$, SP_a, OPO plane; upper right: $\psi_{rot}^{dbl}8$, SP_b, $OPH_{eclipsed}$ plane; lower right: $\psi_{rot}^{dbl}4$, TBP_a, OPH plane.

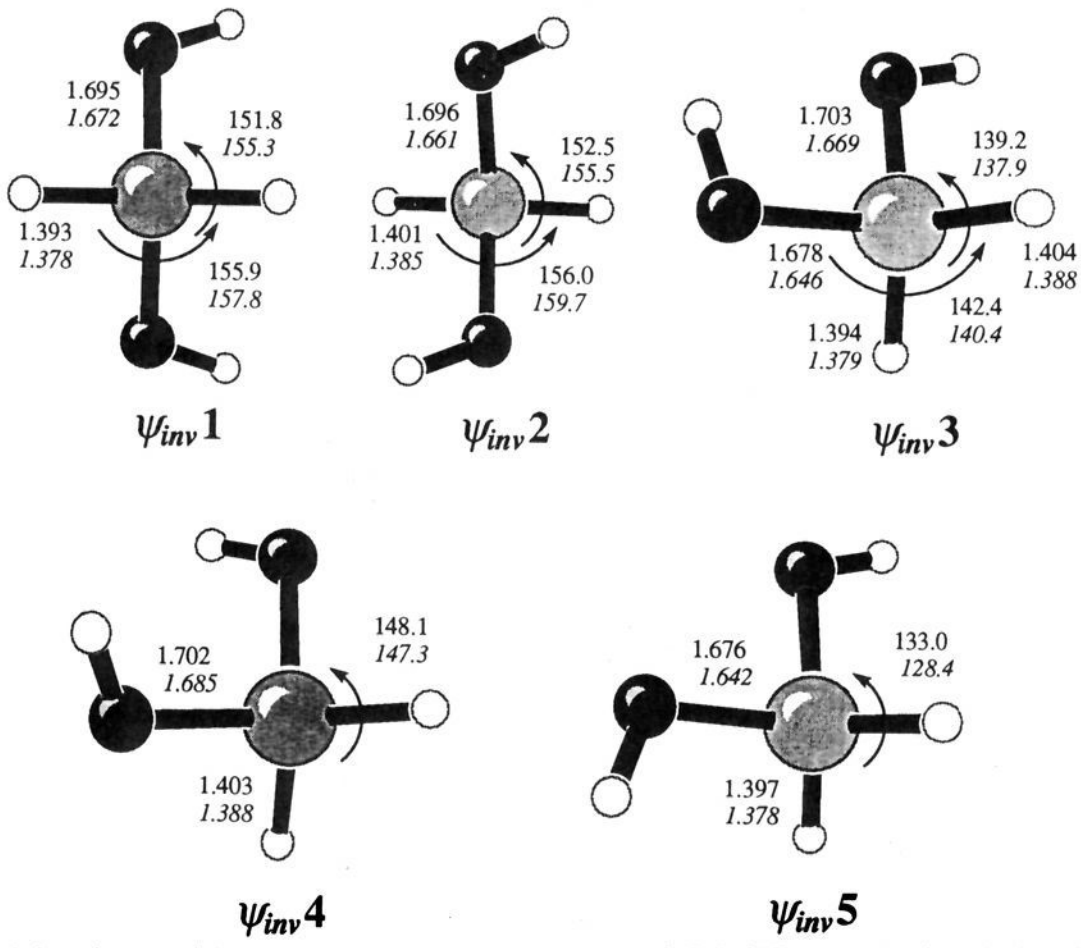

Figure 4. Selected geometrical data for pseudoinversion transition state structures of $H_2P(OH)_2$ optimized at the UMP2 and UHF (italics) levels; bond lengths are in angstroms and bond angles in degrees.

SP_a TS) interchanges both axial substituents with both equatorial. The chief difference is that the unpaired electron does not invert through the central phosphorus atom in this instance. We have located five transition state structures for pseudorotation which are illustrated in Figure 6. The relative energies of $\psi_{rot}1$ and $\psi_{rot}2$ are the lowest of the five; the anti relationship of the hydroxyl groups in the SP base minimizes dipole and steric interactions between them. Of the remaining three TSs, in which the hydroxyl groups are syn, $\psi_{rot}3$ incorporates a nonideal intramolecular hydrogen bond and is thus lower in energy than $\psi_{rot}4$ and $\psi_{rot}5$.

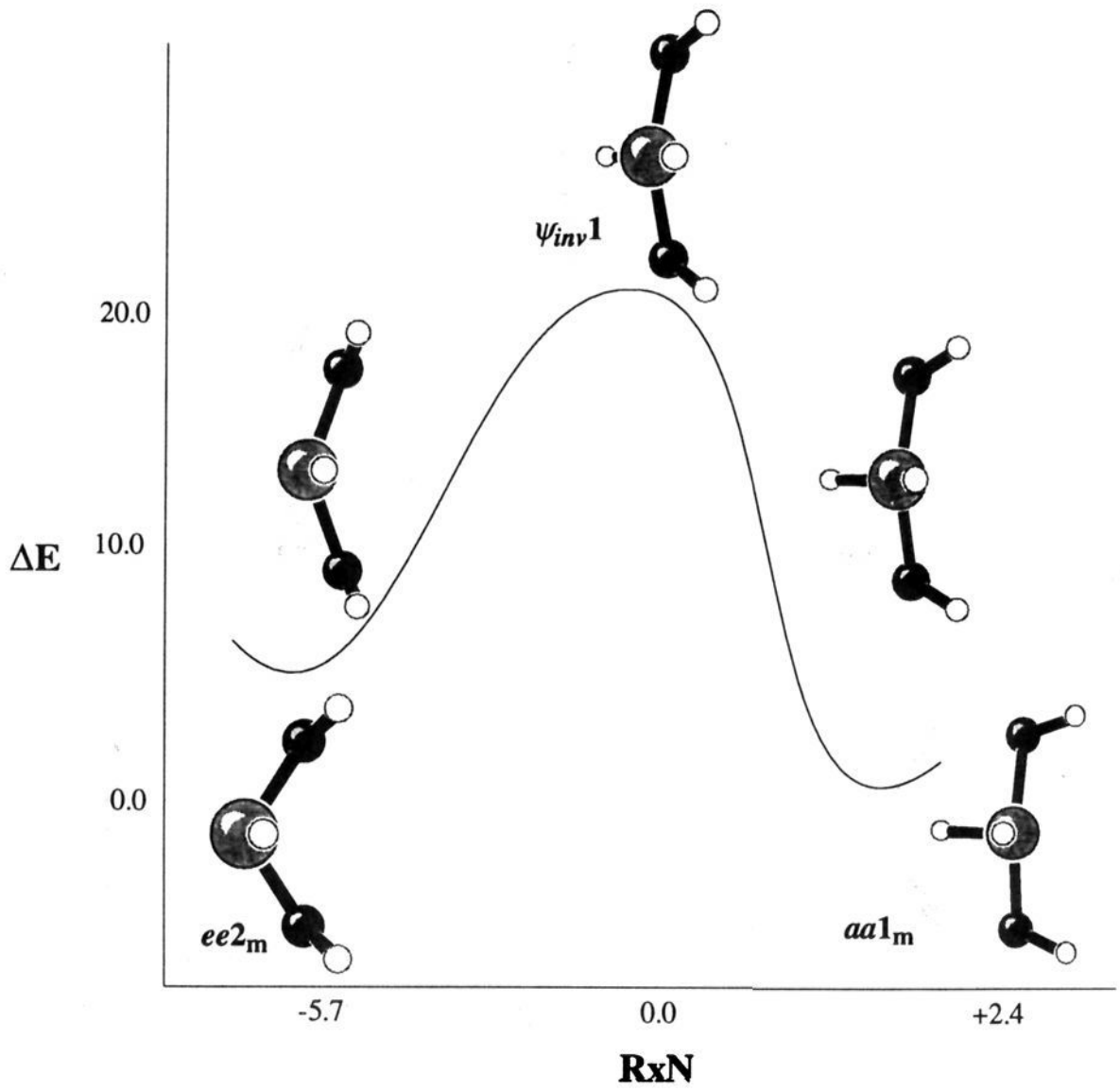

Figure 5. Intrinsic reaction coordinate (in mass scaled internals) linking minima $aa1_m$ and $ee2_m$ via pseudoinversion transition state structure $\psi_{inv}1$.

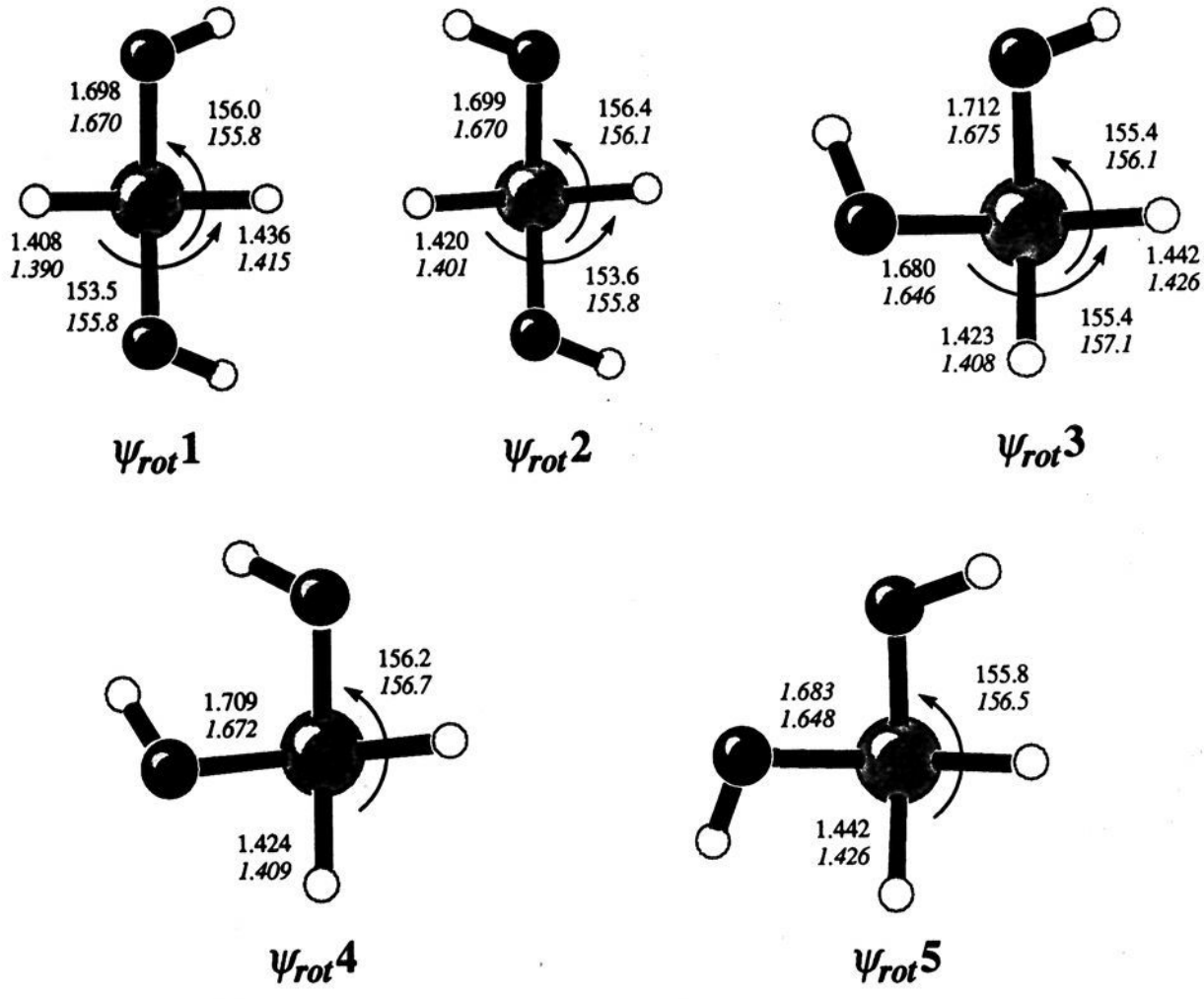

Figure 6. Selected geometrical data for pseudorotation transition state structures of $H_2P(OH)_2$ optimized at the UMP2 and UHF (italics) levels; bond lengths are in angstroms and bond angles in deg.

To illustrate the pseudorotation process, the IRC connecting $aa1_m$ and $ee2_m$ through $\psi_{rot}1$ is provided in Figure 7. Note that Figures 5 and 7 are both IRCs connecting the same two local minima; the difference lies in the nature of the TS. Finally, figure 3 includes a SOMO slice illustrating the SP_a nature of the unpaired electron in $\psi_{rot}1$.

Double Pseudorotation. As mentioned in the introduction, a double pseudorotation is unique in the open-cell case insofar as the net result of the stereopermutation is to exchange only a single equatorial substituent with a single axial one. In an ideal closed shell phosphorane, such a process would require two different, sequential pseudorotations, although recent work by

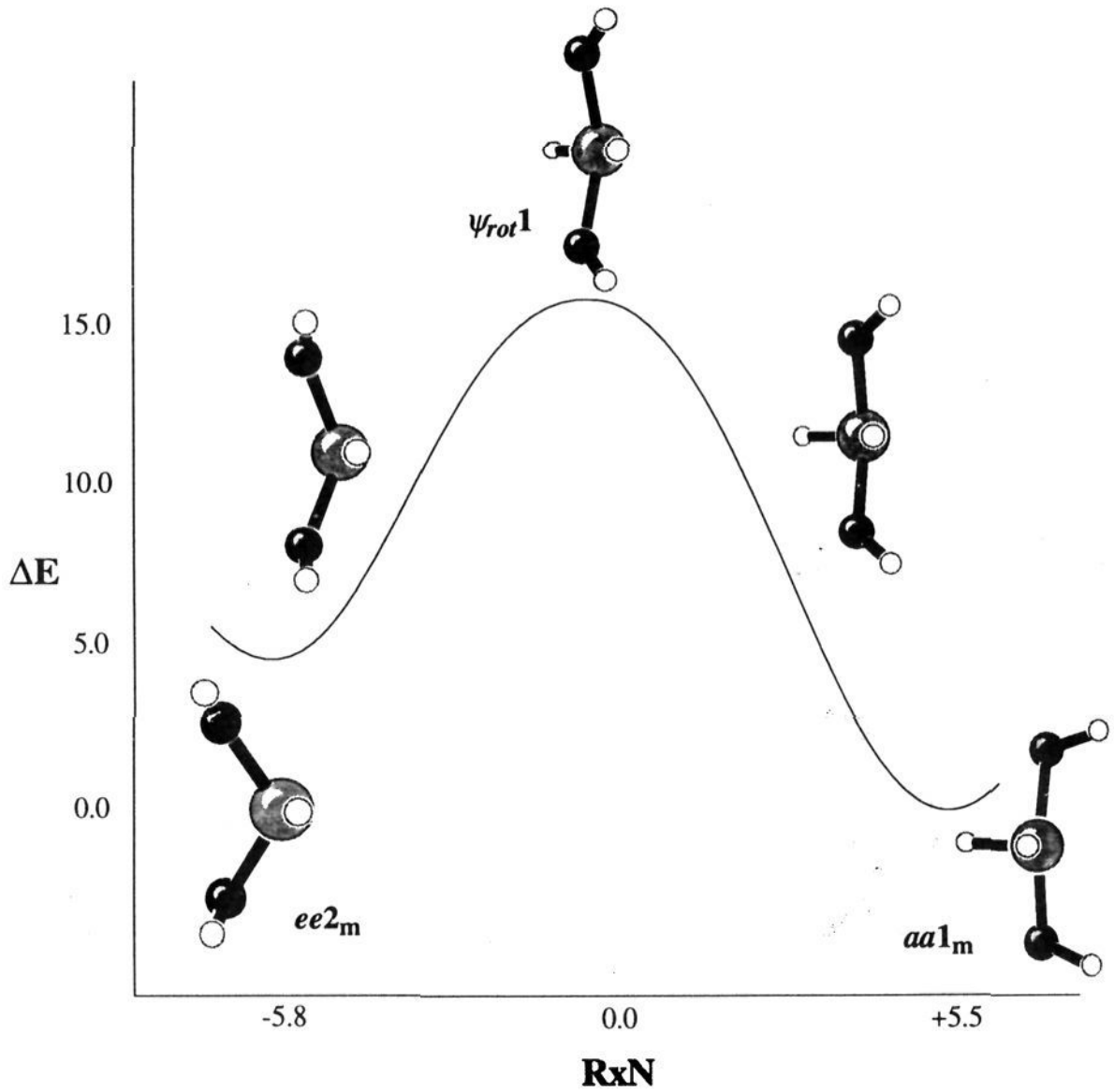

Figure 7. Intrinsic reaction coordinate (in mass scaled internals) linking minima $aa1_m$ and $ee2_m$ via pseudorotation transition state structure $\psi_{rot}1$.

Wasada and Hirao[54] suggests that double-pseudorotation TSs might be locatable for certain phosphoranes with sufficiently apicophobic substituents. We have located ten such transition states for double pseudorotation, and they are illustrated in Figure 8.

For a phosphoranyl radical, the process of double pseudorotation involves following a path from a TBP_e minimum, through an initial SP_b structure, a TBP_a structure, and a second SP_b structure, on the way to the second TBP_e minimum. The TS will be located in the region of the SP_b structure nearest the higher energy local minimum. When the two local minima are identical, e.g., related by the interchange of an axial proton with an equatorial one (a so-called "narcissistic" stereopermutation), then the TS is symmetrically disposed between them. i.e., the TS has a geometry which is more TBP_a-like than SP_b-like. This is illustrated by the two IRCs in Figure 9. The first follows the interconversion of $ae2_m$ to $aa1_m$ via the C_1 SP_b TS $\psi_{rot}^{dbl}8$. The second follows the narcissistic stereopermutation of $ae1_m$ into itself via C_s TBP_a TS $\psi_{rot}^{dbl}4$. Both are relatively low-energy processes, as indeed are all of the double pseudorotations, which range from 8 to 16 kcal/mol above the global minimum. Figure 3 includes SOMO slices for these two TSs and further serves to illustrate the difference in orientations of the unpaired electron.

There are three structural features of particular interest in the double pseudorotation TSs. First, the length of a $P–O_a$ bond is always shorter than a corresponding $P–O_b$ bond by about 0.05 Å. Second, it is evident that if there is a single OH in the X_b position, it prefers to be anti to the unpaired electron. Finally, the basal OH ligands are always rotated perpendicular to the $P–X_a$ bonds, while the apical OH ligands are always rotated so as either to eclipse or be antiperiplanar to the unpaired electron. These constraints suggest that there should be at most 13 possible double pseudorotation TSs. In addition to the ten listed in Figure 8, there are three possibilities in which the two OH groups are basal and anti to each other in the base, *viz.*, both eclipsing the adjacent unpaired electron, both antiperiplanar to the unpaired electron, and one eclipsing/one antiperiplanar. Exhaustive searches of the hypersurface failed to locate any such transition states, which is perhaps unsurprising in light of the above description of the double pseudorotation process and the energetics observed for the true pseudorotation TSs. Although a nonnarcissistic pseudorotation must go through two structures which are SP_b-like in geometry, only the higher energy one will be the transition state. In the pseudorotation series, isomers with anti-basal hydroxyl groups are 5–10 kcal/mol lower in energy than are those with syn-basal hydroxyl groups. As illustrated by the IRC for $\psi_{rot}^{dbl}8$, many double pseudorotations will indeed proceed through SP_b structures with anti-basal hydroxyl groups. However, they will apparently always be lower in energy than the other SP_b structure on the IRC; this is consistent with the observation that they *must* be derived from the aa minima and the double pseudorotation must proceed to a *higher* energy ae minimum.

Bond Homolysis Products. *In order to assess the energetic* stability of $H_2P(OH)_2$, we have finally considered several structures which would result from the dissociation of an H or OH radical from dihydroxyphosphoranyl as shown in eq 1–3. The energies of the products relative to the hydroxyphosphoranyl global minimum are given in Table 1, and the lowest energy structures of OPH_2OH, $PH(OH)_2$, and PH_2OH at the MP2/6-31G* level are presented in Figure 10.

$$PH_2(OH)_2 \rightarrow OPH_2OH + H \quad (1)$$

$$PH_2(OH)_2 \rightarrow PH(OH)_2 + H \quad (2)$$

$$PH_2(OH)_2 \rightarrow PH_2OH + OH \quad (3)$$

Of these three processes, that in eq 1 is the most thermodynamically favorable, although OPH_2OH + H remains 5 kcal/mol

(54) Wasada, H.; Hirao, K. *J. Am. Chem. Soc.* **1992**, *114*, 16.

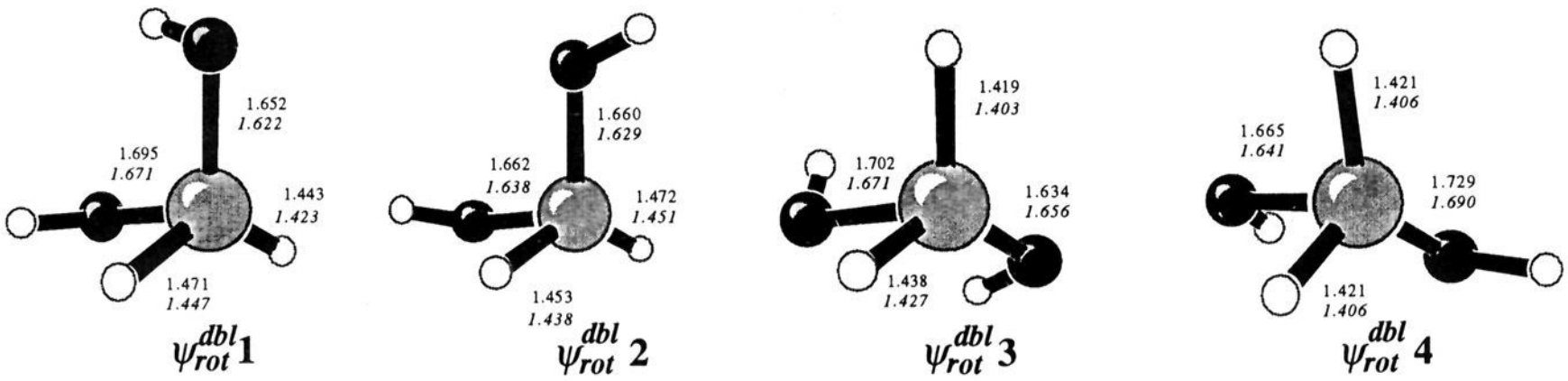

Figure 8. Selected geometrical data for double pseudorotation transition state structures of $H_2P(OH)_2$ optimized at the UMP2 and UHF (italics) levels; bond lengths are in angstroms and bond angles in deg.

higher in electronic energy than $aa1_m$. Since this is about the difference in the MP2 zero point energies (5.8 kcal/mol favoring the right hand side), this suggests that observation of $H_2P(OH)_2$ will only be possible at temperatures so low as to eliminate the additional entropic factors favoring dissociation (assuming there is no intrinsic barrier to homolysis[30]). The overall energy of the dissociative process in eq 2 is 5.3 kcal/mol higher in energy, reflecting the difference in tautomer energies between the two closed-shell H_3PO_2 species. The highly endothermic eq 3 simply illustrates that P–O bonds are quite a bit stronger than P–H.

Discussion

Hyperconjugation in TBP_e Structures. One common approach to identifying the generalized anomeric effect is to analyze bond lengths with respect to the orientation of the delocalizing lone pair. As a rule, delocalization is maximized when the lone pair is antiperiplanar to the X–Y acceptor bond.[6,9,23,24] Such an orientation enjoys a parallel alignment of orbitals, while simultaneously minimizing 4e-destabilizing interactions between the lone pair and the filled σ_{XY} and maximizing overlap with the empty σ^*_{XY} which may have large amplitude outside the bonding region. Since the delocalization is occurring into an antibonding orbital, the bond in question tends to lengthen with increasing hyperconjugation. This trend is well reproduced in the various TBP_e $H_2P(OH)_2$ minima. For instance, in $ee2_m$, the axial P–H bond which is eclipsed by both hydroxyl groups is 0.06 Å longer than is the other axial P–H bond.

This analysis is further borne out by a more careful analysis of the energy difference between the two axial–axial isomers $aa1_m$ and $aa2_m$. Second-order perturbation theory analysis of the Fock matrix in the natural bond orbital (NBO) basis shows that the $n_O \rightarrow \sigma^*_{PH}$ delocalization of the oxygen lone pairs into both of the P–H bonds is more efficient in $aa1_m$ than $aa2_m$, giving rise to the small stabilization of the former relative to the latter. As might be expected, in $aa1_m$, delocalization of oxygen lone pair density into the equatorial P–H bond which is more nearly eclipsed is approximately twice as stabilizing as delocalization into the other P–H bond.

Isomers $ee1_m$ and $ee2_m$ and their associated rotational transition states $ee1^‡$ and $ee2^‡$ provide additional fascinating information about hyperconjugation in the TBP_e system. Although one might assume the O–H bonds to eclipse axial bonds in the TBP in order to maximize delocalization into the associated σ^* orbitals, *it is in fact the equatorial to equatorial* $n_O \rightarrow \sigma^*_{PO}$ *interactions which are maximized by this orientation.* This latter interaction, relative to the idealized Lewis structure, is worth about 17 kcal/mol.[55] In $ee1^‡$ and $ee2^‡$, on the other hand, the stabilization is reduced by about 67%. Similarly, in the rotational transition states, the equatorial to axial $n_{O(e)} \rightarrow \sigma^*_{PH(a)}$ interactions are maximized at about 5 kcal/mol for the HO_ePH_a dihedral angle of 90°. This stabilization is also reduced by about 67% on going to the eclipsed type geometries of the local minima. Given both the greater

(55) Because of the perturbative nature of this analysis, the magnitudes of these energies are best regarded as a qualitative indicator of the importance of hyperconjugation and should not be taken as quantitatively meaningful.

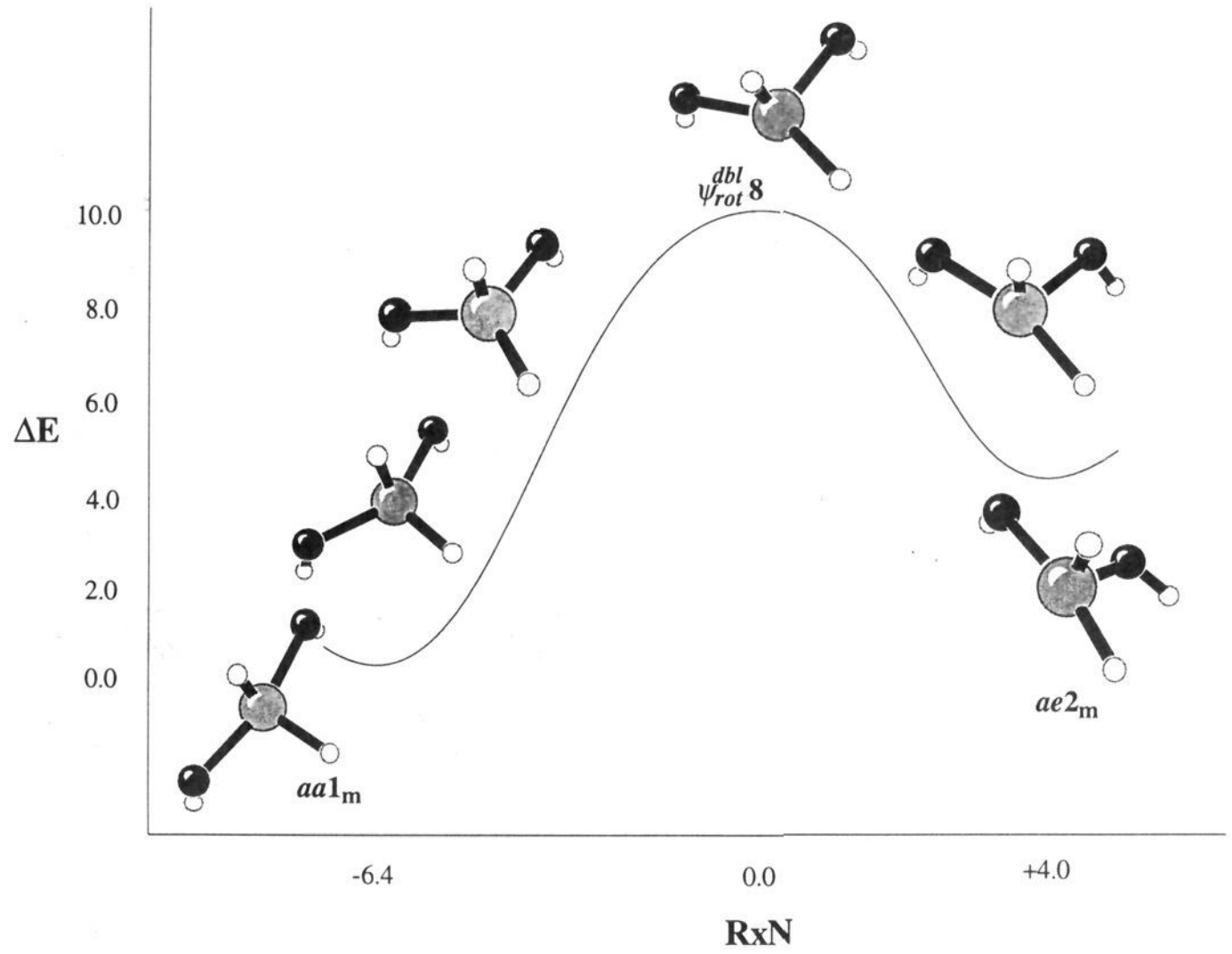

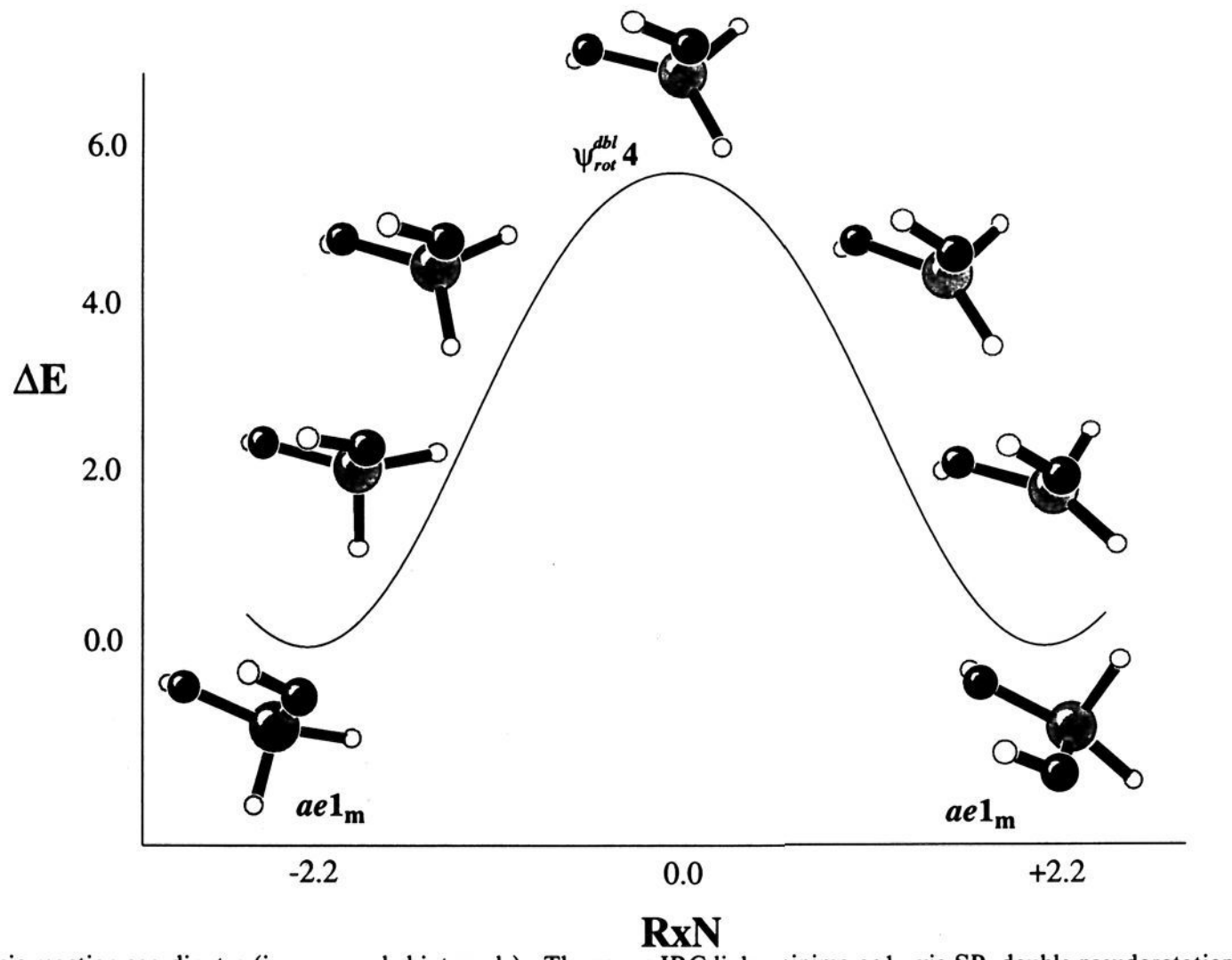

Figure 9. Intrinsic reaction coordinates (in mass scaled internals). The upper IRC links minima $aa1_m$ via SP_b double pseudorotation transition state $\psi_{rot}^{dbl}8$. The lower links two separate permutations of minimum $ae1_m$ via TBP_a double pseudorotation transition state $\psi_{rot}^{dbl}4$.

overlap and the lower energy of the σ^*_{PO} orbitals compared to the σ^*_{PH}, it is unsurprising that n_O delocalization into the former dominates and the hydroxyl groups therefore eclipse the axial P–H bonds in the minimum-energy structures.

The potential-energy surface near the axial–equatorial isomers is more complex and provides a final level of insight into the generalized anomeric effect in these systems. Analogous to the ee surface, the equatorial O–H bond in all minima eclipses either the axial P–O or P–H bond. This is due in part to the fact that the $n_{O(e)} \rightarrow \sigma^*_{PH(e)}$ delocalization is at least twice the magnitude of the $n_{O(e)} \rightarrow \sigma^*_{PH(a)}$ for the identical orientation of oxygen lone pairs. In other words, *interactions between two substituents which are both equatorial are greater than between the same two substituents when either one is axial.*

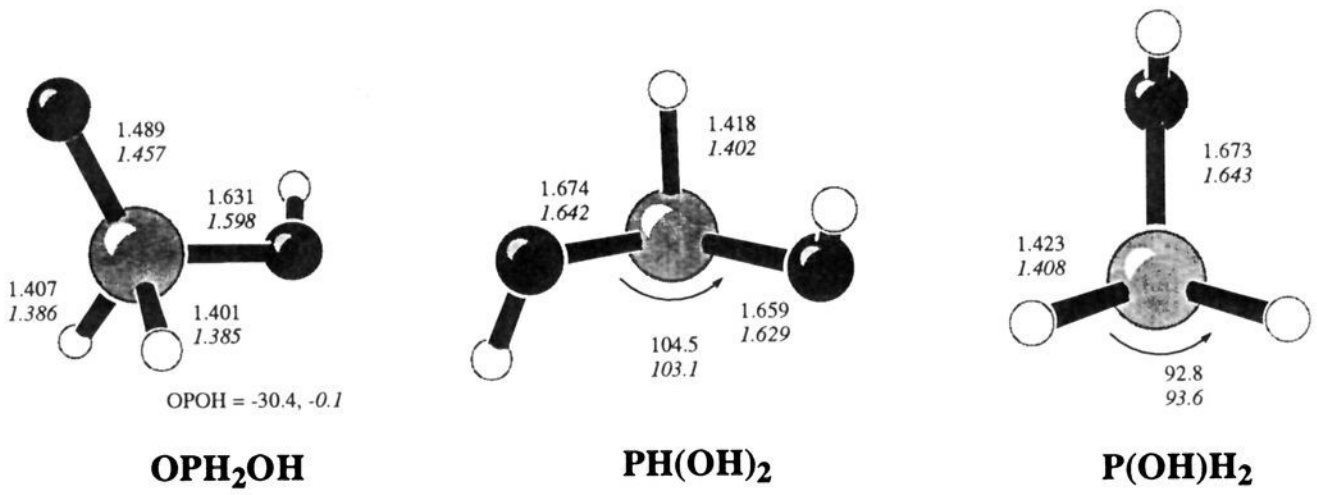

Figure 10. Selected geometrical data for OPH_2OH, $PH(OH)_2$, and $P(OH)H_2$ optimized at the UHF and UMP2 (italics) levels; bond lengths are in angstroms and bond angles in deg.

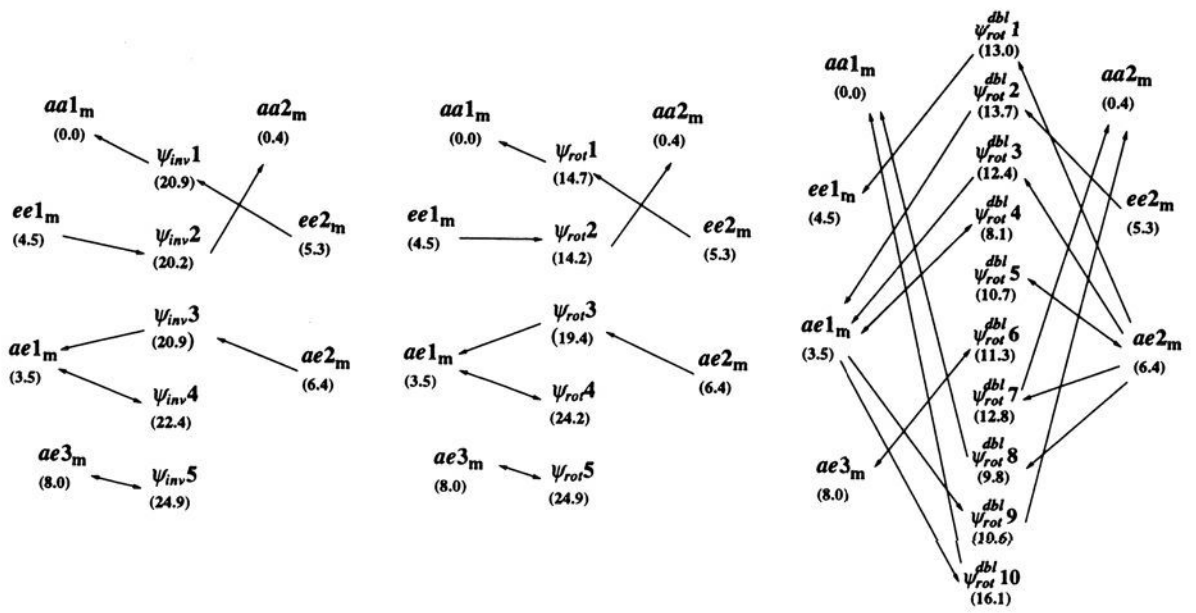

Figure 11. The interconnectivity of the $H_2P(OH)_2$ local minima through all of the pseudoinversion, pseudorotation, and double pseudorotation transition states as determined from IRC calculations. Relative energies are provided for all structures. Single-headed arrows are in the direction of decreasing energy; double-headed arrows indicate a narcissistic process.

This observation agrees with our earlier work in the fluorophosphoranyl series and helps to explain the relationship between hydroxyl apicophilicity and the relative energetics of the aa, ae, and ee local minima in $H_2P(OH)_2$.

Wang and co-workers have investigated apicophilicity in closed-shell phosphoranes for a large number of ligands.[25,26] They found the apicophilicity of OH to be only 0.5 kcal/mol at the MP2/6-31G*//HF/6-31G* level of theory. However, for dihydroxyphosphorane, they found diequatorial substitution to generate the most stable local minimum, which closely resembles $ee1_m$. It is apparent that the stronger equatorial–equatorial hyperconjugative interactions discussed above are operative in the phosphorane series as well and are sufficient to overcome the weak apicophilicity of OH in this system. In contrast, the syn diaxial conformation, $aa1_m$, is the most stable for the dihydroxy phosphoranyl radicals examined here. We have previously shown[27] that the apicophilicity of OH in phosphoranyl radicals is 5.8 kcal/mol at the same level of theory as that used by Wang et al. Evidently, the effect of the unpaired electron in the equatorial position serves to considerably increase the apicophilicity of the hydroxyl ligand. Nevertheless, hyperconjugation is quite evident in stabilizing equatorial hydroxyl substitution in $H_2P(OH)_2$ with interactions not available to H_3POH. Thus, there is only 3.5 kcal/mol energy difference between $aa1_m$ and $ae1_m$ because the 5.8 kcal/mol apicophilicity of the hydroxyl group is offset by stabilizing $n_{O(e)} \rightarrow \sigma^*_{PO(a)}$ hyperconjugation. Moreover, the second movement of an axial hydroxyl to the equatorial position to generate $ee2_m$ costs only 1.8 kcal/mol because the newly available $n_{O(e)} \rightarrow \sigma^*_{PO(e)}$ delocalization is more stabilizing than the $n_{O(e)} \rightarrow \sigma^*_{PO(a)}$ delocalization present in $ae1_m$ as discussed earlier.

Pseudoinversion. Pseudoinversion, which is not available in phosphoranes, is on average the highest energy process for stereopermutation of dihydroxyphosphoranyl isomers. In this process, as illustrated in the IRC of Figure 5, the X_e–P–X_e angle increases and the X_a–P–X_a angle decreases in the direction of the unpaired electron until a flattened, tetrahedral transition state structure is reached. This process continues until the axial substituents become equatorial and vice versa, and the unpaired electron inverts through phosphorus to become localized equatorially on the "opposite side" of the phosphoranyl. We refer to this as pseudoinversion because of the change in the substitution pattern of the TBP ligands, as compared to inversion at a tetrahedral atom, which may change the sense of chirality, but otherwise does not change the *local* stereochemistry. It is often relatively simple to predict the reactants and products corresponding to each of the pseudoinversion transition states. For instance, $\psi_{inv}2$ has an anti arrangement of the hydroxyl groups in the flattened tetrahedron, and thus must interconvert an aa to an ee structure. Moreover, the antiparallel arrangement of the O–H bonds indicates that the minima in question are probably $aa2_m$ and $ee1_m$. That is indeed the case, as verified by an IRC calculation for this process. We have calculated the IRC for all of the pseudoinversion transition states, and a diagram illustrating how they interconvert the various local minima is provided in Figure 11. It appears that for $ae4_m$ no minimum-energy path leads upwards on the hypersurface to a pseudoinversion-like structure. Since $ae4_m$ is only barely stationary at the UHF level, it is likely that any such trajectory merges at some point with the path for $ae2_m$. In any case, $\psi_{inv}1$–$\psi_{inv}5$ appear to span all possible permutations of hydroxyl group location and orientation in the flattened tetrahedron, and exhaustive searching of the hypersurface failed to locate any additional pseudoinversion TSs.

Pseudorotation. As with pseudoinversion, pseudorotation involves an initial increase of the X_e–P–X_e bond angle. However, in the latter process, as illustrated in the IRC of Figure 7, this movement is accompanied not by a *decrease* in the X_a–P–X_a angle, but rather by an *inversion* of this angle through 180°, followed by a decrease in the angle towards the side *opposite* the unpaired electron. The transition-state structure is thus square-pyramidal, with the unpaired electron in the apical position and the four substituents in the basal positions. The bond angles continue to distort until the equatorial and axial substituents have swapped positions in the TBP. The apicophobic unpaired electron thereby remains equatorial. Figure 11 again illustrates how the five psuedorotation TSs interconnect the various local minima as determined by IRC calculations. Again, $ae4_m$ fails to participate, probably because of the nearby location of $ae2_m$, which does connect to $\psi_{rot}3$. The energetics for this process range from 14 to 25 kcal/mol relative to $aa1_m$, consistent with results obtained for monohydroxyphosphorane[26] and -phosphoranyl.[27] As mentioned above, an anti arrangement of the hydroxyl groups in the base of the SP is preferred; such TSs obviously can only connect aa to ee minima.

Double Pseudorotation. The main difference between double and single pseudorotation is that one of the ligands, not the unpaired electron, occupies the apical position in intermediates of SP_b geometry. As illustrated in the IRCs of Figure 9, the apicophobicity of the unpaired electron causes intermediates of TBP_a geometry to be quite high in energy, and the stereopermutation continues to proceed until another TBP_e minimum is reached. The transition state itself is nearest to the higher energy of the two TBP_e minima, with its exact location highly dependent on the energy separation of the two minima. When the process is narcissistic, the TBP_a midpoint becomes the stationary point. This rather complicated overall process is additionally accompanied by rotations of the hydroxyl groups, making if difficult to predict *a priori* the geometries of the reactants and products corresponding to a given transition state. Once again, we have performed IRC calculations for all ten of the double pseudorotation TS structures illustrated in Figure 8, and the manner in which they interconnect the various local minima is diagrammed in Figure 11. The energies of the double pseudorotation TSs range from 8 to 16 kcal/mol above the global minimum. Thus, double pseudorotation is a lower energy stereopermutation than either pseudoinversion or pseudorotation for $H_2P(OH)_2$. This contrasts with the situation in $H_3P(OH)$, where having only a single electron withdrawing substituent allowed pseudoinversion to proceed at lower energy. It is worth noting that, because double pseudorotation exchanges exactly one axial with one equatorial substituent, at least one local minimum on every IRC must be characterized by ae substitution.

Hyperconjugation plays a significant role in stabilizing the double pseudorotation structures as well. For example, in C_s $\psi_{rot}^{dbl}4$, which is TBP_a by virtue of being a TS for the narcissistic stereopermutation of $ae1_m$, the equatorial hydroxyl group is oriented to allow for maximal $n_O \rightarrow \sigma^*_{PH}$ hyperconjugation. This delocalization accounts for a 20 kcal/mol energy lowering relative to the idealized Lewis structure.[55] This effect is also present in the other two C_s symmetric TBP_a TSs, $\psi_{rot}^{dbl}5$ and $\psi_{rot}^{dbl}6$, and they are also relatively low in energy.

ESR Isotropic Hyperfine Coupling Constants. The use of calculated hfs values to assist in the characterization of phosphoranyl radicals is widespread and has, as a rule, been quite successful in terms of agreement between experiment and adequate levels of theory.[28,29,38-44] In general, Fermi contact integrals calculated at either semiempirical or UHF levels are only marginally satisfactory, even in a qualitative sense.[28] Removal of spin contamination, either by using spin annihilated-UHF (PUHF) or UMP2 spin density matrices, affords dramatically improved results which are quantitatively useful. We have tended to prefer the latter and have observed excellent agreement with experiment for a wide variety of radicals, not limited to the phosphoranyl series.[28,29,56-58] We provide as supplementary material the predicted isotropic hyperfine splittings for all local minima calculated at the UMP2/6-311G** level of theory. Calculated infrared frequencies are also provided to potentially assist in experimental identification.

Conclusions

The potential energy hypersurface for $H_2P(OH)_2$ at the correlated level is amazingly complex, with seven local minima, and 29 different transition states arising from four quite different stereopermutational processes. With respect to the minima, analysis of the electronic structures indicates that in addition to standard notions of apicophilicity, relative stability also depends markedly on opportunities for hyperconjugative stabilization. The magnitude of this generalized anomeric effect is greater for the interaction of equatorial substituents than it is for other stereochemical combinations. Interestingly, the tendency for an equatorial hydroxyl group to eclipse axial bonds is not because this maximizes delocalization into three-center acceptor orbitals of the axial system, but rather because it maximizes delocalization into acceptor orbitals in the *equatorial* system. By analysis of the extant data for phosphoranes, this appears to be an entirely general phenomenon, not limited to the open-shell case.

With regard to stereopermutation, hyperconjugation has a significant impact on the hydroxyl group rotational coordinates, especially when they are substituted at the equatorial position. The normal TBP pseudorotational process only occurs through SP transition states in which the unpaired electron occupies the apical position in the SP. This is the lowest energy pathway interconverting aa and ee minima of $H_2P(OH)_2$ *in a single step*. The other single-step alternative, available only for TBP structures in which one of the substituents is an unpaired electron (or a lone pair), is pseudoinversion. Although this is a low-energy pathway for H_3POH, adding an additional hydroxyl group increases the energy of this process sufficiently that it is well above pseudorotation and will probably play no role in phosphoranyl radicals substituted with additional electron-withdrawing groups.

Double pseudorotation, which is dependent on the instability of TBP phosphoranyl radicals in which the unpaired electron is axial, remains a low-energy alternative for interchange of one axial and one equatorial substituent. However, in systems where TBP_a phosphoranyl radicals are stable local minima,[32] thanks to stabilizing hyperconjugative interactions between equatorial substituents, this process becomes less important. This will be the subject of future reports.

Acknowledgment. It is a pleasure to acknowledge support from the U.S. Army Research Office (DAAH04-93-G-0036). We are grateful as well to Dr. Mike Miller for assistance in molecular visualization.

Supplementary Material Available: Predicted ESR and IR spectral data and Gaussian 92 archive information and absolute energies for all structures (12 pages). This material is contained in many libraries on microfiche, immediately follows this article in the microfilm version of the journal, and can be ordered from the ACS; see any current masthead page for ordering information.

(56) Cramer, C. J. *J. Org. Chem.* **1991**, *56*, 5229.
(57) Cramer, C. J. *J. Mol. Struct. (Theochem.)* **1991**, *235*, 243.
(58) Cramer, C. J.; Lim, M. H. *J. Phys. Chem.* Submitted for publication.